ELSEVIER

J. Non-Newtonian Fluid Mech. 104 (2002) 53–63

Journal of Non-Newtonian Fluid Mechanics

www.elsevier.com/locate/jnnfm

Effects of bubble deformation on the viscosity of dilute suspensions

A.C. Rust [a], Michael Manga [b,*]

[a] *Department of Geological Sciences, 1272 University of Oregon, Eugene, OR 97403, USA*
[b] *Department of Earth and Planetary Science, University of California, Berkeley, CA 94720, USA*

Received 15 May 2001; received in revised form 16 October 2001

Abstract

The relative viscosity (μ_{rel} = suspension viscosity/suspending fluid viscosity) of low Reynolds number, dilute and surfactant-free bubble suspensions in simple shear is studied with a rotating cylinder, Couette rheometer. The conditions of the experiments correspond to capillary numbers (*Ca*) of order 1 and bridge previous experimental, theoretical and numerical results that focused on either $Ca \ll 1$ or $Ca \gg 1$. The suspensions are shear thinning with $\mu_{rel} > 1$ for small *Ca*. At large *Ca*, μ_{rel} approaches a constant that is less than 1. These results are explained by a scaling analysis that considers how regions of viscous dissipation in and around bubbles change as bubbles are deformed by the flow.

Keywords: Rheology; Viscosity; Bubbles; Deformation; Dilute suspensions; Emulsions

1. Introduction

In a low Reynolds number shear flow, the rheological properties of a two fluid phase suspension depend on the viscosity and volume fractions of the fluids, microstructures (shape, size, orientation and distribution of the dispersed phase) and interfacial properties (surface tension, concentration and behavior of surfactants). One useful rheological property of suspensions is the relative viscosity, μ_{rel}, defined for simple shear flow as the ratio of the shear viscosity of the suspension (μ) to the shear viscosity of the suspending fluid (μ_s). In a dilute suspension:

$$\mu_{rel} = 1 + f\phi, \tag{1}$$

where ϕ is the volume fraction of the dispersed phase, and f a function that depends on the properties of the suspended particles. For example, Einstein [1] showed that $f = 5/2$ for rigid, spherical particles. Taylor [2] generalized this result for spherical particles of arbitrary viscosity ratio, λ (the ratio of the

* Corresponding author.
E-mail address: manga@seismo.berkeley.edu (M. Manga).

0377-0257/02/$ – see front matter
PII: S0377-0257(02)00013-7

viscosity of the dispersed to the suspending phases), and showed that:

$$f(\lambda) = \frac{5\lambda + 2}{2(\lambda + 1)}. \tag{2}$$

If the dispersed phase is deformable, f also depends on the shape of the particles. If the system is isothermal and surfactant-free so that the surface tension, Γ, is constant, then the magnitude of deformation scales with the capillary number:

$$Ca = \frac{aG\mu_s}{\Gamma}, \tag{3}$$

where G is the shear rate and a the undeformed particle or bubble ($\lambda + 1$) radius. The capillary number is the ratio of shear stresses that deform bubbles to the surface tension stresses that tend to keep bubbles spherical. At the zero shear limit ($Ca \rightarrow 0$), deformable particles remain spherical and the results of Taylor apply (Eq. (2)).

Since bubble deformation produces an anisotropic microstructure, a scalar shear viscosity is not sufficient to describe the suspension viscosity. Theoretical (e.g. [3–5]) and numerical [6] studies show, for example, that large normal stress differences are generated by bubble deformations. In this study, we focus on the relative shear viscosity because it is the pertinent property to calculate the velocity distribution in many commonly encountered situations, such as undirectional flow through a tube or slot. We also consider only steady conditions, i.e. the bubbles have deformed to their steady shapes. The complementary problem for unsteady flows was recently studied experimentally by Llewellin et al. [7] for $Ca \ll 1$ and oscillatory flows.

The rheology of low Re emulsions is relevant to the manufacturing processes involving mixing and extrusion. A further application, and the impetus for the present study, is modeling flow of bubbly magma (silicate melts containing bubbles). Capillary numbers for natural magmatic systems (e.g. volcanic conduits, lava flows) range from $Ca \ll 1$ to $Ca \gg 1$ due to large ranges in melt viscosity and shear rates [8]. Viscosities of bubbly suspensions are best constrained theoretically [5,9,10] and numerically [6,11] at small Ca. Experiments on the rheology of bubble suspensions focus on $Ca \ll 1$, e.g. [12] or $Ca \gg 1$, e.g. [13] though a recently published study by Thompson et al. [14] also considers $Ca = O(1)$. Foams are relatively well studied; however, foam rheology is different from the problem considered here because surfactants play a large dynamic role in foam rheology.

In this study, we bridge the gap between the high and low Ca limits. We use Couette flow experiments to determine the viscosity of low Reynolds number (Re), dilute surfactant-free bubble suspensions under conditions where the relative viscosity is most sensitive to changes in shear rate (Ca=O(1)). We combine these results with experimental data, numerical simulations and theoretical results for higher and lower Ca.

2. Methods

The viscosity of suspensions of deformable bubbles in a viscous, Newtonian fluid is studied using corn syrup as a suspending fluid ($\mu_s = 180$ Pa s at 22 °C) and air bubbles as the dispersed phase. Corn syrup is used because it is nontoxic, water soluble, Newtonian and inexpensive. We assume the syrup is surfactant-free. In experiments on the deformation of air bubbles in corn syrup in simple shear flow [15], we observe no tip streaming and find the shape and orientation of air bubbles in corn syrup agrees with

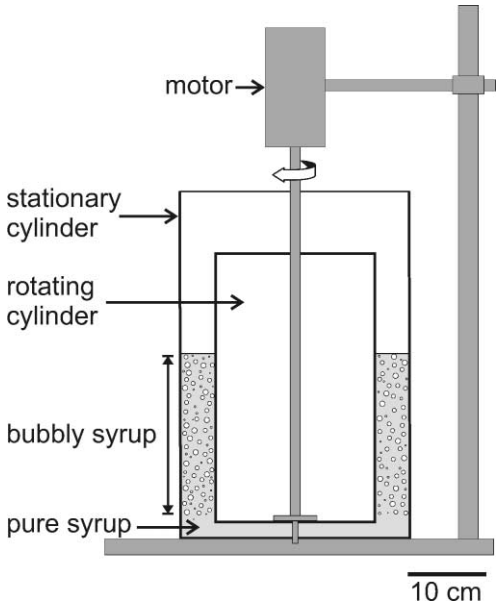

Fig. 1. The Couette flow viscometer.

theoretical predictions (e.g. [16,17]) for a surfactant-free system. Therefore, if surfactants are present they do not significantly influence bubble deformation.

Viscosity measurements are made in a rotating cylinder (Couette) rheometer sketched in Fig. 1. The inner and outer cylinders have a diameter of 20.3 and 29.2 cm, respectively, and are made of transparent acrylic to allow observation of potentially problematic phenomena such as bubble coalescence and large-scale flow patterns. The Reynolds number, based on the shear rate and bubble size, is always $<10^{-5}$. To simplify the subtraction of end effects, the lower gap between the cylinders is filled with bubble-free syrup for which viscosity is independent of shear rate. Viscosities of bubbly corn syrup as a function of rotation rate are determined by subtracting the torque associated with the gap-filling syrup (determined before adding bubbly syrup) from measurements of the torque required to rotate the inner cylinder immersed in bubbly syrup underlain by bubble-free syrup. Relative viscosities are determined by comparing the torque required to shear the annulus of bubbly syrup to the torque to shear an annulus of the same height of bubble-free syrup at the same shear rate and temperature. Temperature corrections are based on measurements with a Cole Parmer® 98936 series rotational viscometer of corn syrup viscosity at multiple temperatures.

Emulsions (e.g. Fig. 2) are formed by the mechanical mixing and breakup of air bubbles injected into corn syrup. Compressed air enters the syrup from the end of a hollow, rotating shaft with a propeller blade at the end. The propeller breaks the emerging air bubbles into numerous bubbles as the shaft rotates and is moved through the syrup, stirring it. We determine the bubble volume fractions (ϕ) from the bulk density measurements of the pure and bubbly corn syrups and present results for $\phi = 0.035$, 0.115, and 0.163. Large ϕ are difficult to achieve presumably because of the lack of surfactants.

The incorporation of bubbles into the syrup may cause changes in water content, and thus viscosity of the suspending fluid (μ_s). To reduce systematic errors from water content, temperature and fluid

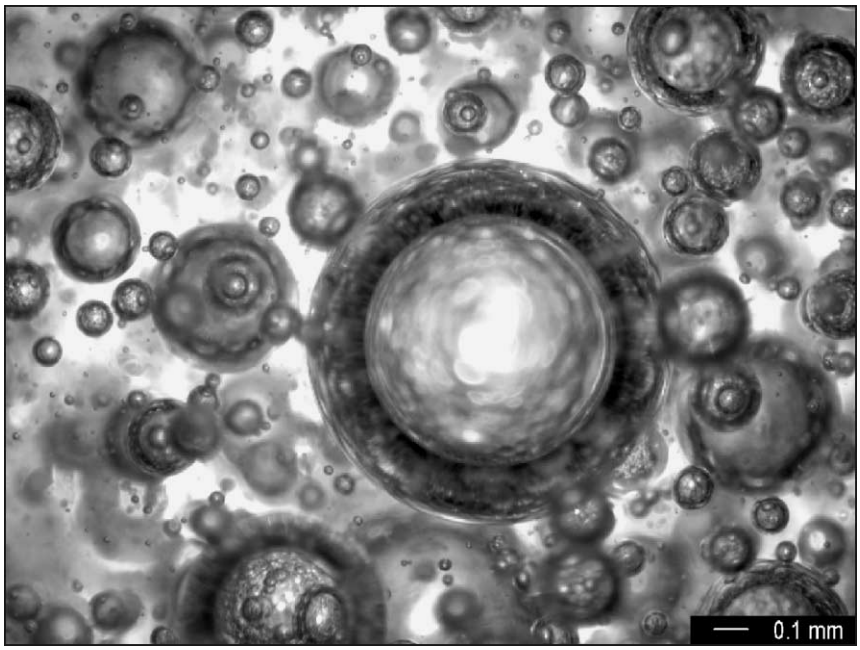

Fig. 2. Photomicrograph of corn syrup with 16% air bubbles by volume. Note the range in bubble sizes. The large bubble in the center is the largest bubble imaged.

heights, we adjust the μ_s value for each experiment so that μ_{rel} approaches the zero-shear limit ($\mu_{rel,0}$) based on the Kreiger–Dougherty [18] equation:

$$\mu_{rel} = \left(1 - \frac{\phi}{\phi_m}\right)^{-f\phi_m}, \tag{4}$$

where ϕ_m is the maximum packing fraction of bubbles and f, the intrinsic viscosity, is the same function that appears in Eq. (1). For these calculations we use $\phi_m = 0.6$ and $f = 1$ [2]. Numerical simulations for $Ca \ll 1$ (presented later) agree with the predictions of the Kreiger–Dougherty equation for the range of ϕ considered in this study.

As the syrup contains a range in bubble sizes (Fig. 2) and shear rates vary radially in the rheometer, we define a characteristic capillary number, denoted Ca^*, using the shear rate, G_i, at the wall of the inner (rotating) cylinder and a characteristic bubble radius, a^*, i.e.:

$$Ca^* = \frac{G_i a^* \mu_s}{\Gamma}. \tag{5}$$

The characteristic bubble radius, a^*, is determined from:

$$a^* = \frac{\sum_{i=1}^{n} a_i^3}{\sum_{i=1}^{n} a_i^2} = \frac{\sum(\text{bubble radius})(\text{bubble area in photo})}{\sum \text{bubble area in photo}}, \tag{6}$$

where a_i is the radius of the ith bubble. Bubble sizes are measured from multiple digital photographs (1600 × 1200 pixels) taken at 100× and 40× magnification under a microscope. The number of bubbles

measured ranges from 150 to 300. A volume averaged bubble radius is the most appropriate average to define a characteristic radius [19]. We use a photograph area average in Eq. (6) because the probability of imaging a given bubble is proportional to its radius. Values of a^* are 0.24, 0.29 and 0.26 mm for the experiments with $\phi = 0.035$, 0.115 and 0.163, respectively. All bubbles are at least an order of magnitude smaller than the gap between the cylinders of the rheometer.

Our relative viscosity measurements are limited to $Ca^* < 3$ due to complications related to viscous dissipation and bubble coalescence at high shear rates. Higher shear rates require greater strains to achieve steady bubble shapes. Large strains lead to viscous dissipation and as a result, a reduction in the viscosity of the suspending fluid as the temperature rises. Here, the fluid temperature changes by less than 0.2 °C for each set of measurements at a given ϕ.

Large strains also change the emulsion textures because of greater numbers of bubble–bubble interactions. In preliminary experiments, significant coalescence occurred at high shear rates, as evidenced by a reduction in the height of the bubbly fluid due to new, large bubbles rising to the upper surface. Observations on individual bubbles in the syrup-filled rheometer indicate that bubble migration is not significant on the time scales and shear rates of the experiments (see also [20]).

Measurements for determining viscosity as a function of shear rate are made at progressively increasing shear rates. At each shear rate, once the apparatus torque and shear rate appear steady, measurements are made over a period of tens of seconds. Returning to lower shear rates after completion of the experiments reproduces the results suggesting that the size and spatial distribution of the bubbles does not change. We do not observe the hysteresis that Vinckier et al. [21] attribute to changing droplet size. Capillary numbers are sufficiently small that bubbles do not break [22].

3. Results

As expected, the relative viscosity, μ_{rel}, depends on both the volume fraction of bubbles, ϕ, and the capillary number, Ca (Figs. 3 and 4). Suspensions are shear thinning and $\mu_{\text{rel}} > 1$ for small Ca^*, and $\mu_{\text{rel}} < 1$ for Ca^* greater than about 0.5. That is, the viscosity of the suspension is greater than that of the suspending fluid at low shear rates where the bubbles remain nearly spherical due to surface tension. At shear rates that are high enough to significantly deform bubbles, bubbles reduce the viscosity of the mixture. As ϕ increases, μ_{rel} becomes increasingly sensitive to changes in shear rate (G); however, we are able to discern shear-thinning rheology at ϕ as low as 0.035.

We compare our data with two theoretical equations developed by Frankel and Acrivos [9] and Han and King [10] relating relative viscosity and Ca (Fig. 3b). Both equations assume that bubbles are only slightly deformed and are relevant to dilute and semi-dilute suspensions, respectively. For $\lambda = 0$, the Frankel and Acrivos equation is:

$$\mu_{\text{rel}} = \frac{1 + ((6/5)\text{Ca})^2 + \phi(1 - (12/5)\text{Ca}^2)}{1 + ((6/5)\text{Ca})^2}. \tag{7}$$

The Han and King model which is based on Choi and Schowalter [5] is:

$$\mu_{\text{rel}} = \frac{1 + ((6/5)\text{Ca})^2(1 + (20/3)\phi)(1 + 4\phi)}{1 + ((6/5)\text{Ca})^2(1 + (20/3)\phi)^2}(1 + \phi + \tfrac{5}{2}\phi^2), \tag{8}$$

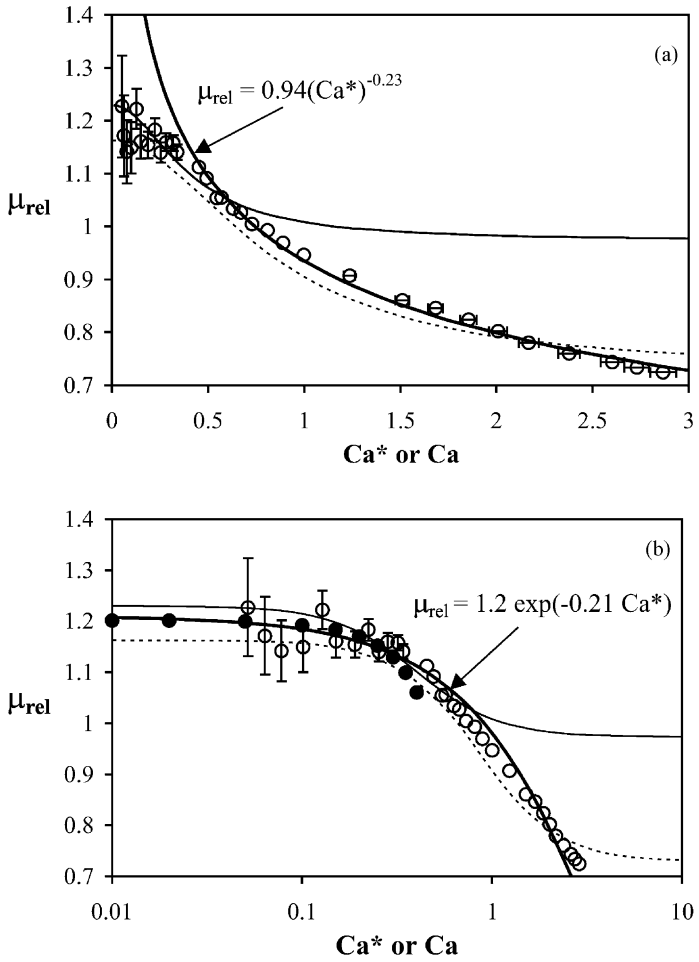

Fig. 3. Relative viscosity as a function of characteristic capillary number (experimental data) or capillary number (numerical simulation data and theoretical model curves) for bubbly corn syrup with 16.3% air bubbles. Experimental and numerical data are represented by open and filled circles, respectively. One standard deviation error bars are given for experimental data with errors greater than the symbol size. A power law curve (a) fits the experimental data well except at low Ca^* where an exponential curve (b) is better (thick black lines). The discrepancy between the numerical and experimental data suggests that Ca^* overestimates Ca. Also plotted, are the theoretical predictions of Frankel and Acrivos [9] (dashed line) and Han and King [10] (thin solid line) based on small deformation theories (see text for details).

for $\lambda = 0$. Both theoretical equations describe the experimental data well for $Ca < 1$ (Fig. 3b). Given that the models are based on small deformation theories, it is not surprising they are less accurate at high Ca. For $Ca > 1$, the Han and King relationship greatly overpredicts the suspension viscosity. The Frankel and Acrivos model is much closer to the experimental data. As $Ca \to \infty$, the Frankel and Acrivos equation reduces to Eq. (1) with $f = -5/3$ which is the solution for spherical, inviscid inclusions in the limit of no surface tension [23,24].

We also compare our experimental data with numerical simulations of monodisperse suspensions of ordered bubbles (Fig. 3). The numerical simulation methods are identical to those of Manga and

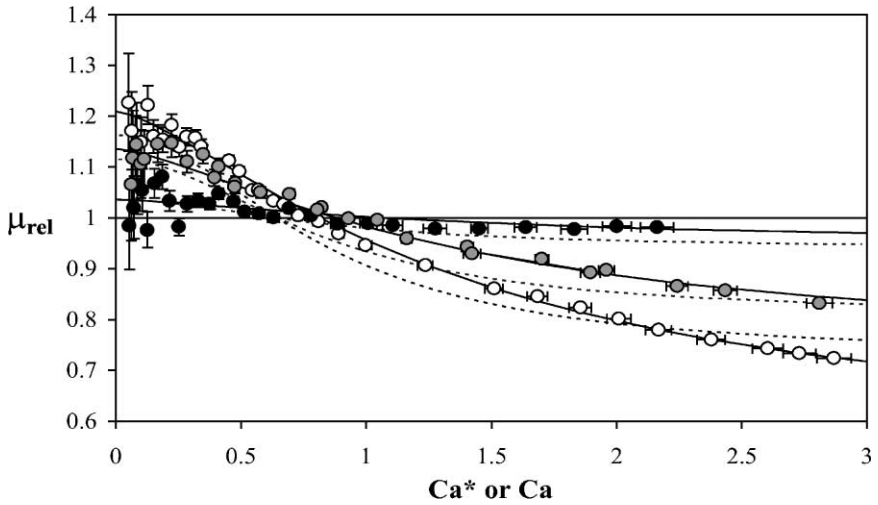

Fig. 4. Relative viscosity as a function of characteristic capillary number for bubbly corn syrup with 3.5% (black), 11.5% (grey), and 16.3% (white) air bubbles. Error bars are same as in Fig. 3. The horizontal line $\mu_{rel} = 1$ is the relative viscosity of pure (bubble-free) syrup. The set of solid curves plotted are derived from simultaneously fitting the Cross equation (Eq. (9)) to the three data sets ($\phi = 0.035$, 0.115 and 0.163). We set $\mu_{rel,0}$ to the Kreiger–Dougherty equation (Eq. (4)) $Ca \ll 1$ limit ($\phi_m = 0.6$ and $f_0 = 1$) and set $\mu_{rel,\infty} = 1 + c_1\phi + c_2\phi^2$. The best least-squared residual fit is $K = 0.72$, $m = 1.43$, $c_1 = -1.14$, and $c_2 = -9.80$. The dashed curves are theoretical predictions of Frankel and Acrivos [9] for the three bubble volume fractions of the experiments.

Loewenberg [25] and are based on the boundary integral method technique described in Loewenberg and Hinch [6]. Calculations are limited to $Ca \leq 0.4$ because more deformed bubbles develop pointed ends with curvature that cannot be adequately resolved numerically. The numerical results are similar to the experimental data but predict lower μ_{rel} at the largest Ca (e.g. Fig. 3b). A possible source of this disparity is an overestimate of all Ca^* due to employing the shear rate at the inner cylinder which is the highest shear rate in the fluid. The experimental data would also be shifted into agreement with the numerical results by using different a^* or Γ (we use 0.080 N/m from [26]). We should not necessarily expect perfect agreement between the numerical and experimental data sets, however, because the corn syrup-bubble suspensions are unordered and contain a range of bubble sizes (Fig. 2).

Since numerical solutions are limited to low Ca and there are only analytical solutions for the shape of bubbles at $Ca \ll 1$ [27] and $Ca \gg 1$ [28], we also fit our data with empirical equations. A power-law model fits the μ_{rel} (Ca) data well except at very low G (i.e. low Ca), where an exponential model fits the data better (Fig. 3). To fit the data to a single empirical curve we use the Cross [29] equation, which has been shown to fit viscosity data as a function of stress or strain rate for suspensions of 'squishy' spheres [30] such as blood [31] and aqueous dispersions of polymer latex spheres [32]. We use a modified Cross equation given by:

$$\mu_{rel} = \mu_{rel,\infty} + \frac{\mu_{rel,0} - \mu_{rel,\infty}}{1 + (K\,Ca^*)^m}, \tag{9}$$

where $\mu_{rel,0}$ and $\mu_{rel,\infty}$ refer to the asymptotic values of relative viscosity at very low and very high shear rates, respectively, and K and m are dimensionless constants.

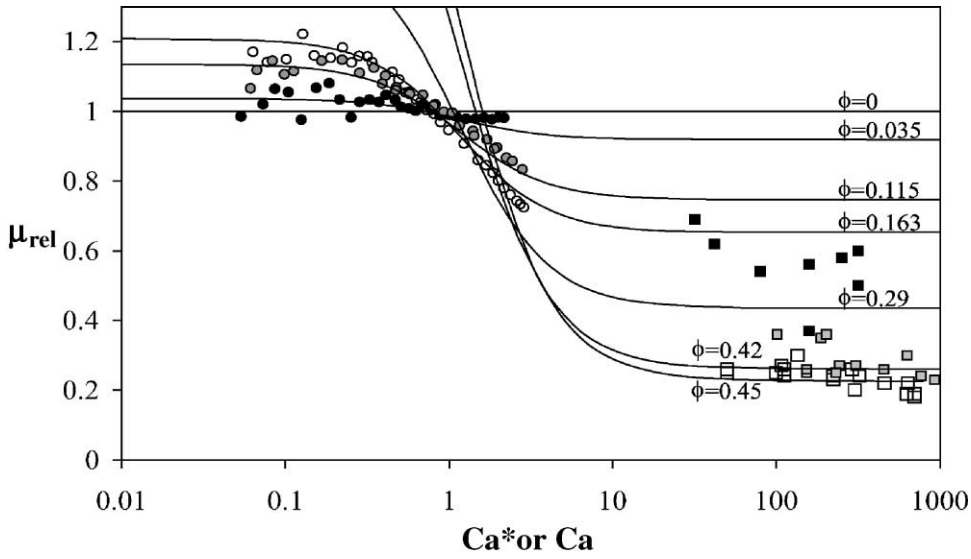

Fig. 5. Relative viscosity as a function of characteristic capillary number for bubbly corn syrup and bubbly silicate melt. The symbols for our syrup experiments (circles) are the same as in Fig. 4. The black, grey and open squares correspond to bubbly silicate melt experiments with $\phi = 0.29$, 0.42 and 0.45, respectively, of Stein and Spera [13]. The three bubbly syrup data sets ($\phi = 0.35$, 0.115 and 0.163) are simultaneously fit to the Cross equation (Eq. (9)) as in Fig. 4. However, in this case, $\mu_{\mathrm{rel},\infty}$ is estimated with the Krieger–Dougherty equation (Eq. (4)) with $\phi_m = 0.9$, the maximum packing for cylinders, to allow extrapolation to non-dilute suspensions. The best-fit parameters are $K = 0.86$, $m = 1.61$, and $f_\infty = -2.37$. The high *Ca* limits are in reasonable agreement with the Stein and Spera data despite not including the latter in the curve fitting analysis.

To produce a general equation describing μ_{rel} as a function of *Ca* and ϕ, we simultaneously fit the Cross equation to the three data sets ($\phi = 0.35$, 0.115 and 0.163). We set $\mu_{\mathrm{rel},0}$ to the Kreiger–Dougherty equation (Eq. (4)) $Ca \ll 1$ limit ($\phi_m = 0.6$ and $f_0 = 1$) and set $\mu_{\mathrm{rel},\infty} = 1 + c_1\phi + c_2\phi^2$. Solving for K, m, c_1 and c_2, the best least-squared residual fit is $K = 0.72$, $m = 1.43$, $c_1 = -1.14$, and $c_2 = -9.80$. The resulting set of curves fits the data well (Fig. 4) but it is clearly not applicable to non-dilute suspensions because $\mu_{\mathrm{rel},\infty}$ is negative for $\phi > 0.27$.

To extrapolate the Cross equation to higher ϕ, we apply the Krieger–Dougherty equation (Eq. (4)) with $\phi_m = 0.9$, the maximum packing for cylinders to estimate $\mu_{\mathrm{rel},\infty}$. We must also determine the high shear rate intrinsic viscosity, $f(Ca \to \infty) \equiv f_\infty$, as well as, K and m in the Cross equation (Eq. (9)). The best-fit parameters are $K = 0.86$, $m = 1.61$ and $f_\infty = -2.37$. For comparison, $f = -5/3$ for spherical, inviscid inclusions in the limit of no surface tension [23,24] and the Frankel and Acrivos [9] equation approaches this solution at high *Ca*. In Fig. 5 we plot the resulting Cross equation curves along with data from Stein and Spera [13] for bubbly, surfactant-free, silicate melts ($\mu_s = 10^{6.4}$–$10^{8.6}$) and $\phi = 0.29$, 0.42 and 0.45. The experiments performed by Stein and Spera are restricted to large *Ca*. The high *Ca* limits of the Cross equation fits based on the Krieger–Dougherty equation with $\phi_m = 0.9$ are in reasonable agreement with the higher ϕ measurements of Stein and Spera [13], despite not including the latter in the best fit analysis. The Frankel and Acrivos equation also fit the Stein and Spera data despite being based on small deformations in dilute suspensions.

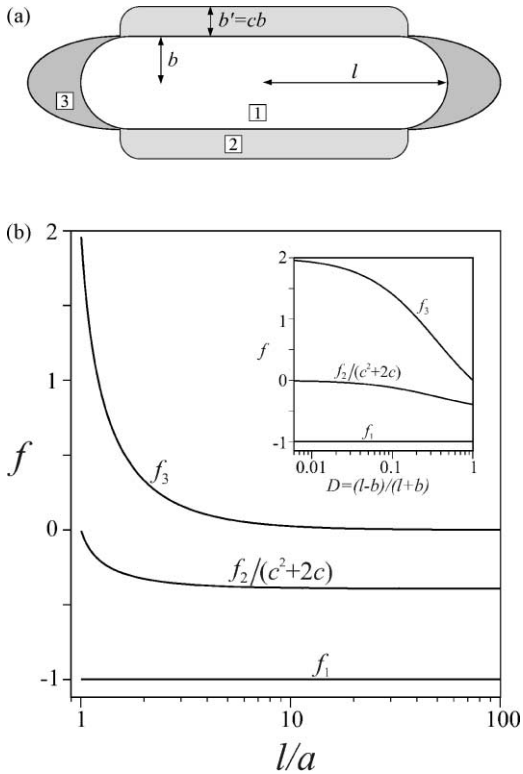

Fig. 6. (a) Three regions in and around bubbles that contribute to viscous dissipation in a sheared bubbly suspension. In regions 1 and 2, dissipation is reduced relative to that in the undisturbed simple shear flow. In region 3, dissipation is enhanced; (b) Contributions to the intrinsic viscosity, f in Eq. (1), from regions 1, 2 and 3 (f_1, f_2, and f_3, respectively) as a function of bubble deformation (l/a or D). See text for details.

4. Discussion

In principle, from knowledge of the bubble shape and flow field, the relative viscosity can be calculated. Unfortunately, while there are analytical solutions describing the shape of bubbles for both $Ca \ll 1$ [22] and $Ca \gg 1$ [23], there is no general solution appropriate for $Ca = \mathrm{O}(1)$. Thus, here we develop scaling estimates that will help provide an insight into the three distinctive aspects of the rheological measurements: (1) suspensions with small Ca, $0 < Ca < \mathrm{O}(1)$, are shear thinning; (2) for small Ca, the relative viscosity is greater than 1; (3) at greater Ca, the relative viscosity approaches a constant value less than 1.

We model bubbles as cylinders with hemispherical caps (Fig. 6a) and consider viscous dissipation in three volumes: (1) the bubble, (2) a deformed annulus of suspending fluid around the cylindrical portion of the bubble, and (3) suspending fluid around the spherical caps of the bubble. Each of these regions contributes to the intrinsic viscosity of the suspension, f (see Eq. (1)), and:

$$f = f_1 + f_2 + f_3, \tag{10}$$

where the subscripts correspond to the contributions from the three volumes defined above and in Fig. 6.

For inviscid bubbles, viscous dissipation only occurs in the suspending phase, which occupies a volume fraction of $1-\phi$. If we neglect effects of flow around bubbles, the replacement of viscous fluid by inviscid bubbles in a given volume reduces the relative viscosity from $\mu_{rel} = 1$ to $\mu_{rel} = 1-\phi$. Therefore, $f_1 = -1$ for all bubble shapes.

Viscous dissipation in fluid around a bubble (volumes 2 and 3, Fig. 6) depends on the shape of the bubble. We characterize the bubble deformation by $D = (l - b)/(l + b)$ or l/a where l and b are the semi-major and semi-minor axes of the bubble, respectively, and a is the radius of the undeformed bubble. In a low *Re* simple shear flow, $D \approx Ca$ for $Ca \ll 1$ [22] and $l/a \propto Ca^{1/2}$at $Ca \gg 1$ [23].

Since the fluid–fluid interface at bubble margins is a free slip surface, velocity gradients are reduced near the bubble and thus, there is less viscous dissipation in the annulus around the cylindrical portion of a bubble (region 2, Fig. 6) than there would be if there was no bubble. Therefore, $f_2 \leq 0$. The magnitude of f_2 scales with the volume of region 2 which is a distorted cylindrical annulus. The characteristic thickness of the annulus, b', is set to $b' = cb$, where b is the semi-minor axis of the bubble and c is an unknown constant. In Fig. 6 we normalize f_2 by dividing by $(c^2 + 2c)$, which is proportional to the volume of the annulus. Spherical bubbles ($D = 0$ and $l/a = 1$) have no cylindrical portions and thus, $f_2 = 0$. A value proportional to the volume of the bubble (assumed to be constant).

Streamlines in a simple shear flow field are deformed and deflected around bubbles resulting in greater viscous dissipation around the caps of the bubbles (i.e. $f_3 > 0$). For spherical bubbles with free slip surfaces, $f_3 = 2$ [2]. With increasing bubble deformation, f_3 decreases and approaches zero at $Ca \gg 1$ because highly deformed bubbles cause very little deflection of flow lines.

The variations in f_1, f_2, and f_3 illustrated in Fig. 6 demonstrate why bubble suspensions are shear-thinning, $\mu_{rel} > 1$ at $Ca \ll 1$, $\mu_{rel} < 1$ at $Ca \gg 1$ and μ_{rel} approaches a constant value at $Ca \gg 1$. Relative viscosities greater than 1 are dominated by the increased viscous dissipation around slightly deformed bubbles ($Ca \ll 1$). Relative viscosities less than 1 at high Ca result from decreased viscous dissipation due to free slip surfaces, augmented by reduced volume fraction of viscous fluid due to the presence of inviscid bubbles. The rheology is shear thinning because the volume of fluid with reduced viscous dissipation (region 2) increases with greater bubble deformation. Furthermore, the volume with increased viscous dissipation (region 3) decreases as bubbles become more deformed. For highly deformed bubbles, dissipation in region 3 is negligible, the volume of fluid in region 2 approaches a constant, and thus the relative viscosity approaches a constant for $Ca \gg 1$.

Acknowledgements

This work was supported by NSF grant EAR0003303 and a NSERC PGSB award. D. Senkovich, K. Johnson and C. Dax provided technical assistance. We thank D. Stein and F. Spera for sharing their unpublished data.

References

[1] A. Einstein, Eine neue Bestimmung der Molekuldimensionen, Ann. Phys. 19 (1906) 289–306; English translation in Investigation on the Theory of Brownian Motion, Dover, New York, 1956.

[2] G.I. Taylor, The viscosity of a fluid containing small drops of another fluid, Proc. R. Soc. London, Ser. A 138 (1932) 41–48.

[3] W.R. Schowalter, C.E. Chaffey, H. Brenner, Rheological behaviour of a dilute emulsion, J. Coll. Interf. Sci. 26 (1968) 152–160.
[4] D. Barthès-Biesel, A. Acrivos, Deformation and burst of a liquid droplet freely suspended in a linear shear field, J. Fluid Mech. 61 (1973) 1–21.
[5] S.J. Choi, W.R. Schowalter, Rheological properties of nondilute suspensions of deformable particles, Phys. Fluids 18 (1974) 420–427.
[6] M. Loewenberg, E.J. Hinch, Numerical simulation of a concentrated emulsion in shear flow, J. Fluid Mech. 321 (1996) 395–419.
[7] E.W. Llewellin, H.M. Mader, D.R. Wilson, The rheology of a bubbly liquid, J. Royal Soc., London Ser. A., in press.
[8] M. Manga, J. Castro, K.V. Cashman, M. Loewenberg, Rheology of bubble-bearing magmas, J. Volc. Geotherm. Res. 87 (1998) 15–28.
[9] N.A. Frankel, A. Acrivos, The constitutive equation for a dilute emulsion, J. Fluid Mech. 44 (1970) 65–78.
[10] C.D. Han, R.G. King, Measurement of the rheological properties of concentrated emulsions, J. Rheol. 24 (1980) 213–237.
[11] X. Li, H. Zhou, C. Pozrikidis, A numerical study of the shearing motion of emulsions and foams, J. Fluid Mech. 286 (1995) 379–404.
[12] H.M. Princen, A.D. Kiss, Rheology of foams and highly concentrated emulsions: IV An experimental study of the shear viscosity and yield stress of concentrated emulsions, J. Coll. Interf. Sci. 128 (1989) 176–187.
[13] D.J. Stein, F.J. Spera, Shear Viscosity of rhyolite-vapor emulsions at magmatic temperatures by concentric cylinder rheometry, J. Volc. Geotherm. Res., in press.
[14] M.J. Thompson, J.R.A. Pearson, M.R. Mackley, The effect of droplet extension on the rheology of emulsions of water in alkyd resin, J. Rheol. 45 (2001) 1341–1358.
[15] A.C. Rust, M. Manga, Bubble shapes and orientations in low Re simple shear flow, in press.
[16] G.I. Taylor, The formation of emulsions in definable fields of flow, Proc. R. Soc. London, Ser. A 146 (1934) 501–523.
[17] E.J. Hinch, A. Acrivos, Long slender drops in a simple shear flow, J. Fluid Mech. 98 (1980) 305–328.
[18] I.M. Kreiger, T.J. Dougherty, A mechanism for non-Newtonian flow in suspensions of rigid spheres, Trans. Soc. Rheol. 3 (1959) 137–152.
[19] D. Graebling, R. Muller, J.F. Palierne, Linear viscoelastic behavior of some incompatible polymer blends in the melt. Interpretation of data with a model of emulsion of viscoelastic liquids, Macromolecules 26 (1993) 320–329.
[20] M.R. King, D.T. Leighton, Measurement of shear-induced dispersion in a dilute emulsion, Phys. Fluids 13 (2001) 397–406.
[21] I. Vinckier, M. Minale, J. Mewis, P. Moldenaers, Rheology of semi-dilute emulsions: Viscoelastic effects caused by the interfacial tension, Coll. Surf. A 150 (1999) 217–228.
[22] H.P. Grace, Dispersion phenomena in high viscosity immiscible fluid systems and application of static mixers as dispersion devices in such systems, in: Proceedings of the 3rd Engineering Foundation of Research Conference Mixing, Andover NH, 1971; republished in Chem. Eng. Commun. 14 (1982) 225–277.
[23] J.M. Dewey, The elastic constants of materials loaded with non-rigid fillers, J. Appl. Phys. 18 (1947) 578–581.
[24] J.D. Eshelby, The determination of the field of an ellipsoidal inclusion and related problems, Proc. R. Soc. London, Ser. A 241 (1957) 376–396.
[25] M. Manga, M. Lowenberg, Viscosity of magmas containing highly deformable bubbles, J. Volc. Geotherm. Res. 105 (2001) 19–24.
[26] A. Borhan, J. Pallinti, Breakup of drops and bubbles translating through cylindrical capillaries, Phys. Fluids 11 (1999) 2846–2855.
[27] G.I. Taylor, The formation of emulsions in definable fields of flow, Proc. R. Soc. London, Ser. A 146 (1934) 501–523.
[28] E.J. Hinch, A. Acrivos, Long slender drops in a simple shear flow, J. Fluid Mech. 98 (1980) 305–328.
[29] M.M. Cross, Rheology of non-Newtonian fluids: a new flow equation for pseudo-plastic systems, J. Coll. Sci. 20 (1965) 417–437.
[30] J. Mewis, W.J. Frith, T.A. Strivens, W.B. Russel, The rheology of suspensions containing polymerically stabilized particles, AIChE 35 (1989) 415–422.
[31] P. Mills, J.M. Rubi, D. Quemada, Suspension flow, in: G. Astarita, G. Marrucci, L. Nicolais (Eds.), Rheology, Vol. 2: Fluids, Plenum Press, New York, 1980, pp. 127–147.
[32] D. Quemada, Rheology of concentrated disperse systems, Rheol. Acta 17 (1978) 643–653.